ChemistrySelect

Research Article
doi.org/10.1002/slct.202303381

Chemistry Europe
European Chemical Societies Publishing

www.chemistryselect.org

Synthesis, Characterization, and Biological Activity of Di-2-pyridyl Ketone Aryl Hydrazone and Its Copper(II) Complex and the Interaction of Di-2-pyridyl Ketone Aryl Hydrazone with DNA Bases

Murat Çınarlı,*[a] Esin Kıray,[a] and Çiğdem Yüksektepe Ataol[b]

The development of antibiotic resistance has also increased the interest in hydrazones. In this paper, we describe the new aroyl hydrazone and its Cu(II) complex, which we synthesized. Aroyl hydrazone (HL) was prepared by the condensation reaction of 3-hydroxy-2-naphthoic hydrazide with di-2-pyridyl ketone. Ligand (HL) and its transition metal complexes [CuL_2] (1), have been characterized by elemental analysis, FT-IR, UV-Vis., ^{1}H-NMR, and LC–MS techniques. The molecular structure of HL, whose crystal structure could not be obtained, was elucidated by the DFT/B3LYP/6-311+G(d, p) method. The optimized molecular structure, total energy, molecular orbital energy values, molecular electrostatic potential map, reactivity parameters, and interaction with DNA bases were investigated. Theoretical UV-vis spectra of HL were obtained with TD-DFT in different solvent environments. In addition, the ligand and its complex were examined for their antimicrobial activity against pathogenic microorganisms by using a minimal inhibitory concentration method (MIC). It was determined that the [CuL_2] (1) complex was generally moderately active. It was also observed that the [CuL_2] (1) complex was more active than the HL.

Introduction

The development of drug resistance to clinically used anti-infective agents reveals that there is an urgent need for the discovery of new antimicrobial compounds to treat multi-resistant infections.[1–2]

The coordination chemistry of modified hydrazones has been an important field of study due to the remarkable anticancer, antibacterial, and antimicrobial activities exhibited by these compounds and metal complexes.[3–8] Polydentate hydrazones are important scaffolds that exhibit multidisciplinary applications such as DNA binding and cleavage, antimicrobial, antifungal, catalytic effects, and chemospecific reactants.[9–16] Aroyl hydrazones are recognized by the general formula (RC (H)=N-NR_1R_2) and can be considered a good class of polydentate. In addition, groups such as OH, C=O and NH_2 that aryl hydrazones have increase their binding effect to various metal ions.[17] Considering the significant effects of aroyl hydrazones and polydentate hydrazones and similar studies,[18–21] new polydentate aroyl hydrazone (HL) and its Cu(II) complex (1) derived from 3- hydroxy-2-naphthoic acid hydrazide and di-2-pyridyl ketone have been synthesized to establish their possible antibacterial and antifungal activity. The synthesized compounds were characterized by elemental analysis, FT-IR, UV-Vis., ^{1}H-NMR, LC–MS techniques. The molecular structure of HL was elucidated with the Density Functional Theory (DFT) by selecting the B3LYP base function and the 6-311+G(d, p) basis set. The bond parameters were obtained by optimizing the molecular structure in both gas and methanol, DMSO, and water solvent environments and compared with the values in the literature. By using optimized structures, single point energy calculation of HL was made, total energy, molecular orbital energy values, molecular electrostatic potential map (MEP), global reactivity parameters, and theoretical UV-vis spectra by using Time-Dependent (TD) DFT were obtained to investigate the interaction with DNA bases such as adenine (AN), guanine (GN), cytosine (CN) and thymine (TN). All were examined for antimicrobial activities against pathogenic type strains (Gram-negative and Gram-positive bacteria) and clinical isolates.

Results and Discussion

^{1}H-NMR spectrum of (HL)

The ^{1}H-NMR spectrum of the ligand showed a characteristic singlet signal for the NH group at δ 13.90 ppm. The single signal of the OH group of the ligand was observed at 11.28 ppm. The spectrum of the ligand shows multiple signals in the range of 7.48–8.86 ppm, which are characteristic signals for aromatic ring protons (Figure 1).[22,23]

[a] Dr. M. Çınarlı, Dr. E. Kıray
Ahi Evran University, Vocational School of Health Services, Kırşehir, Turkey
E-mail: murat.cinarli@ahievran.edu.tr

[b] Prof. Dr. Ç. Y. Ataol
Çankırı Karatekin University, Faculty of Science, Department of Physics, 18100, Çankırı, Turkey

Supporting information for this article is available on the WWW under https://doi.org/10.1002/slct.202303381

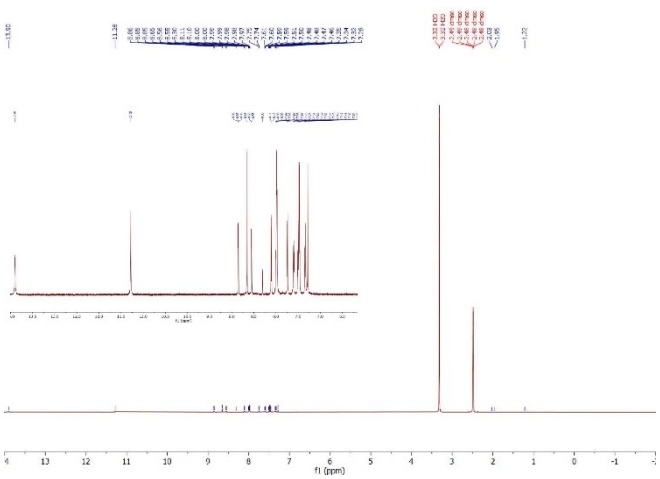

Figure 1. ^{1}H-NMR spectrum of the HL.

FTIR studies of (HL) and (1)

In the IR spectrum of **HL**, the bands at 3284 cm^{-1} and 3253 cm^{-1} are due to υ(N–H) and υ(O–H), respectively. The υ(N–H) band was not observed in the complex spectrum. The OH band was observed at 3233 cm^{-1} in the complex **1** spectrum. This indicates that the NH group is coordinated with the metal ion and the OH group is uncoordinated. The IR spectrum of the ligand shows three absorption bands at 1676, 1628, and 1521 cm^{-1} due to ν(C=O), $\nu(C{=}N)_{azo}$, and $\nu(C{=}N)_{pyr}$, respectively. The IR spectrum of the complex reveals significant changes compared to this of the ligand. While the ν(C=O) band was not observed in the complex **1** spectrum, the ν(C–O) bands were recorded at 1362 cm^{-1}. In the complex spectrum, the $\nu(C{=}N)_{azo}$ and $\nu(C{=}N)_{pyr}$ bands were recorded at 1638 and 1509 cm^{-1}, respectively. In addition new bands due to the conjugate system ν (>C=N–N=C<) appeared at 1584 cm^{-1} (Figure 2).[22–24] These spectral changes in the complex concerning the ligand are related to the involvement of these groups in coordination.

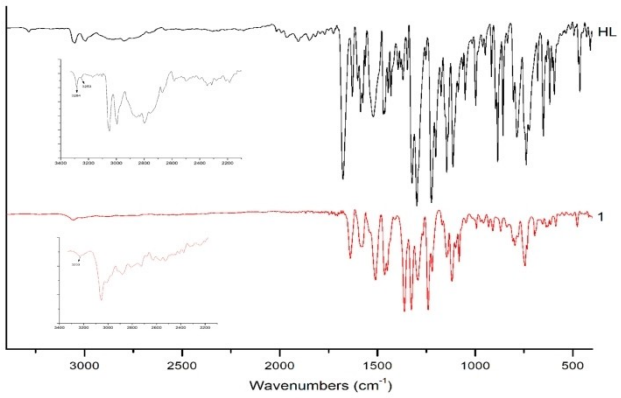

Figure 2. FT-IR spectra of the **HL** and **1**.

The geometric optimization studies of the molecular structure of (HL)

The molecular structure of the $C_{22}H_{16}N_4O_2$ (HL) compound, which consists of functional groups such as naphthalene, hydrazine, carbonyl, and pyridine, was investigated by the DFT method, which is one of the theoretical calculation method. The B3LYP base function, which is one of the hybrid function that gives good results in exchange-correlation energy in organic compounds, is included in the calculations. In the calculations, 6-311 + G(d, p) was chosen as the polarized diffuse basis set. The molecular structure of the $C_{22}H_{16}N_4O_2$ compound was optimized in the gaseous environment in the ground state and different solvent environments with a dielectric constant (ε) and dipole moment (μ) (Methanol (ε = 32.7, μ = 1.7), DMSO (ε = 46.7, μ = 3.9), and Water (ε = 80.1, μ = 1.82). In the calculations, methanol medium, DMSO, and water environments in which the compound was dissolved experimentally were chosen as solvents. The optimized molecular structure of $C_{22}H_{16}N_4O_2$ compound obtained by the B3LYP/6-311 + G(d, p) method in ground state water medium is given in Figure 3.

By using optimized structures obtained from four different media, the bond parameters of the molecular structure were obtained and a list of some bond parameters is given in Table 1.

The C(3)-O(15) bond length in the naphthalene group of the compound was found to be 1.36990 Å in the gaseous environment and 1.37071 Å in the water environment. In the literature, this bond distance is given 1.355(3) Å according to the experimental X-ray diffraction analysis results and as 1.351 Å in the water environment according to the theoretical calculation results.[25] The bond distance of the C(11)-O(12) carbonyl group was found as 1.21573 Å in gas < 1.22473 Å in methanol < 1.22497 A in DMSO < 1.22520 Å in water media. These values are close to the values in the literature.[26] The N(14)-C(16) bond distance in the hydrazine group was found to be 1.288 Å on average, with a double bond character. When these values are compared with the literature, it can be said that the results found are slightly different.[26,27] When the results obtained from gas and solvent environments are compared, it is seen that

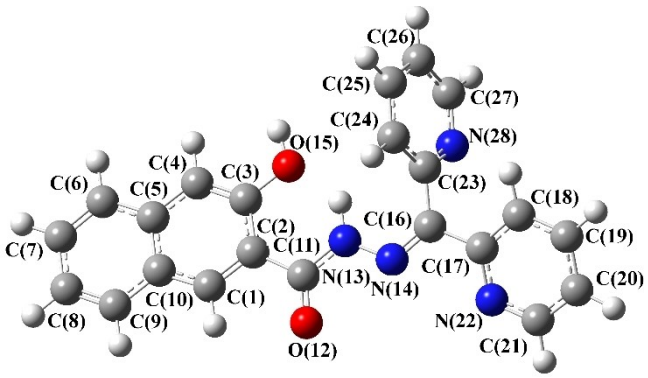

Figure 3. The optimized molecular structure of the $C_{22}H_{16}N_4O_2$ compound obtained by the B3LYP/6-311 + G(d, p) method in ground state water medium.

Table 1. The bond parameters of the $C_{22}H_{16}N_4O_2$ by using DFT/B3LYP/6-311+G(d, p).

	B3LYP/6-311+G (d, p) Gas	B3LYP/6-311+G (d, p) Methanol	B3LYP/6-311+G (d, p) DMSO	B3LYP/6-311+G (d, p) Water
Bond Lenghts (Å)				
C(3)-O(15)	1.36990	1.37094	1.37083	1.37071
C(11)-O(12)	1.21573	1.22473	1.22497	1.22520
C(11)-N(13)	1.38925	1.37774	1.37759	1.37745
N(13)-N(14)	1.34254	1.35691	1.35695	1.35696
N(14)-C(16)	1.29453	1.28800	1.28803	1.28804
C(16)-C(17)	1.49715	1.49020	1.49020	1.49023
C(16)-C(23)	1.48948	1.50359	1.50356	1.50355
C(17)-N(22)	1.34081	1.34523	1.34534	1.34544
N(22)-C(21)	1.33655	1.33323	1.33328	1.33332
C(23)-N(28)	1.34611	1.34305	1.34309	1.34312
N(28)-C(27)	1.33462	1.33708	1.33712	1.33716
Bond Angles (°)				
O(15)-C(3)-C(2)	117.613	118.051	118.046	118.040
C(3)-C(2)-C(11)	126.746	126.731	126.715	126.701
C(2)-C(11)-O-(12)	120.627	121.105	121.109	121.113
C(2)-C(11)-N-(13)	116.803	116.581	116.587	116.594
O(12)-C(11)-N-(13)	122.491	122.303	122.294	122.283
C(11)-N(13)-N-(14)	117.676	119.695	119.696	119.694
N(13)-N(14)-C(16)	122.738	118.847	118.852	118.861
N(14)-C(16)-C(17)	113.108	117.686	117.687	117.687
N(14)-C(16)-C(23)	126.402	124.067	124.057	124.048
C(16)-C(23)-N-(28)	116.971	116.171	116.152	116.133
C(16)-C(17)-N-(22)	117.645	117.918	117.926	117.932
Torsion Angles (°)				
O(15)-C(3)-C(2)-C(11)	−0.158	0.302	0.335	0.371
C(3)-C(2)-C(11)-O(12)	161.425	−172.470	−172.491	−172.502
C(3)-C(2)-C(11)-N(13)	−21.735	8.701	8.662	8.638
C(2)-C(11)-N-(13)-N(14)	177.644	−177.470	−177.557	−177.646
O(12)-C(11)-N-(13)-N(14)	−5.580	3.716	3.611	3.508
C(11)-N(13)-N-(14)-C(16)	170.894	−177.900	−177.946	−1777.999
N(13)-N(14)-C(16)-C(17)	177.531	−177.573	−177.605	−177.641
N(13)-N(14)-C(16)-C(23)	−4.236	2.703	2.643	2.579
N(14)-C(16)-C(17)-N(22)	−153.327	19.743	19.565	19.410
N(14)-C(16)-C(23)-N(28)	25.024	−111.636	−111.473	−111.316

N(14)-C(16)-C(17)-N(22) and N(14)-C(16)-C(23)-N(28) torsion angles found to be quite different. The structural geometry of the molecular structure differs in this region.

The energy studies of the molecular structure of (HL)

By using the optimized molecular structure of the $C_{22}H_{16}N_4O_2$ compound, a single point energy calculation was made with the B3LYP/6-311+G(d, p) method in the ground state gas, methanol, DMSO, and water environments. Molecular orbital (MO) energy values, total energy, dipole moment, and global reactivity parameters of the molecular structure were obtained by single-point energy calculation. Levels of the highest molecular orbital HOMO, filled by electrons, and the lowest molecular orbital LUMO, not filled by electrons, can determine the chemical activity parameters of a molecule. The greater the difference between the HOMO and LUMO energy levels (ΔE), the more chemically reactive the molecular orbital is and hard. The smaller this difference, the less an electron in the HOMO level of the molecular structure can switch and the more chemically active the molecular structure is. The molecular orbital energy values, total energies, dipole moment (μ), and ΔE range of the $C_{22}H_{16}N_4O_2$ are given in Table 2. As can be seen from Table 2, HOMO and LUMO energy levels decreased in solvent environments compared to the gas environment of the molecular structure. Molecular structure of −1217.75309 a.u. it has been found that it has the lowest value in the water environment with its total energy value and is more stable in this environment than the others.

Electron density (Figure 4) and molecular electrostatic potential (MEP) (Figure 5) maps of the molecular structure were obtained by single point energy calculation by using the B3LYP/6-311+G(d, p) method in the ground state. MEP map helps us to understand the attractive and repulsive potential regions in the molecular structure and enables us to determine which regions of the molecular structure are active in intermolecular bonds. The red regions on the map represent nucleophilic regions and the blue regions represent electrophilic regions.

As can be seen from the MEP map of the $C_{22}H_{16}N_4O_2$, mostly, hydrazine nitrogen, pyridine nitrogen and carbonyl oxygen atoms of the molecular structure are nucleophilic, while naphthalene oxygen hydrogen is electrophilic.

Table 2. The molecular orbital energy values, total energies, dipole moment, and ΔE range of the $C_{22}H_{16}N_4O_2$ (96MO).

$C_{24}H_{24}N_6OS_2$	E_{HOMO} (eV)	E_{LUMO} (eV)	Total energy (a.u)	μ (D)	ΔE (eV)
B3LYP/6-311 + G(d, p) Gas	−6.09594	−2.18591	−1217.73536	4.7929	3.91003
B3LYP/6-311 + G(d, p) Methanol	−6.27119	−2.37448	−1217.75194	12.2727	3.89671
B3LYP/6-311 + G(d, p) DMSO	−6.27228	−2.38210	−1217.75254	12.3729	3.89018
B3LYP/6-311 + G(d, p) Water	−6.27336	−2.38945	−1217.75309	12.4678	3.88391

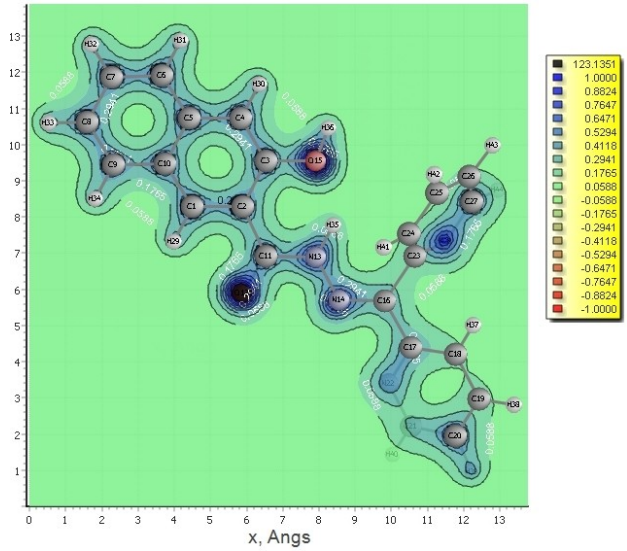

Figure 4. The electron density map of the $C_{22}H_{16}N_4O_2$ by using the B3LYP/6-311 + G(d, p) in water media.

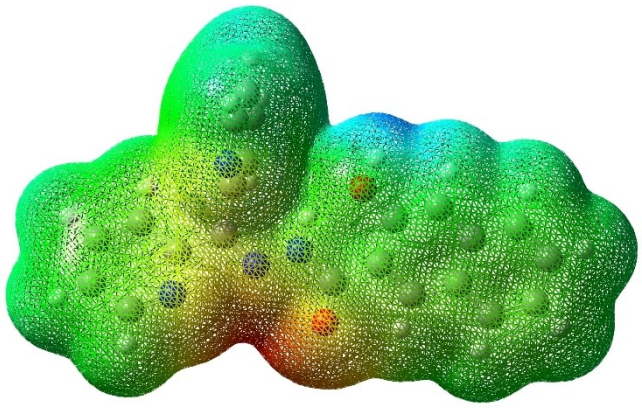

Figure 5. The MEP map of the $C_{22}H_{16}N_4O_2$ by using the B3LYP/6-311 + G(d, p) in water media.

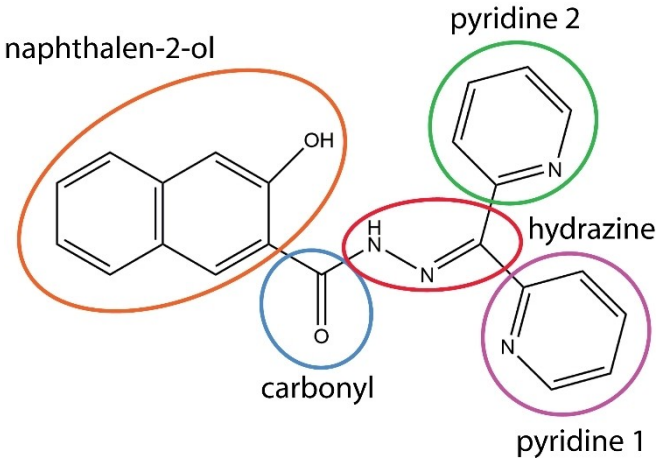

Figure 6. The parts of the $C_{22}H_{16}N_4O_2$.

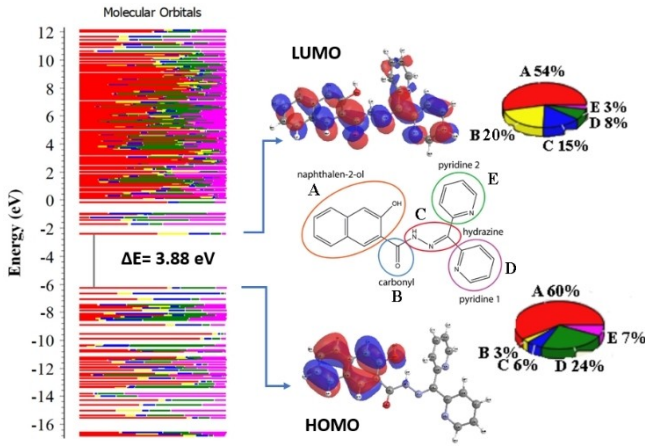

Figure 7. The % atomic contributions of the groups to these levels and the molecular orbital energy levels of the molecular structure by using the B3LYP/6-311 + G(d, p) in water media.

The naphthalene-2-ol part of the molecular structure seen in Figure 6 can be defined as A, the carbonyl group as B, the hydrazine group as C, the pyridine 1 group as D, and the pyridine 2 group as E.

The % atomic contributions of these groups to the molecular orbital energy levels of the molecular structure were obtained by single point energy calculation and are given in Figure 7.

Figure 7 shows the energy bands of the molecular structure. Within these energy bands, the distribution of π bonding and π* antibonding molecular orbitals corresponding to HOMO (96thMO) and LUMO (97thMO) levels, as well as the percentage of atomic contributions of functional groups in the molecular structure to these levels are given.

The highest contribution to the HOMO energy level came from the electrons of naphthalene > pyridine 1 > pyridine 2 > hydrazine > carbonyl groups and to the LUMO level from the electrons of naphthalene > carbonyl > hydrazine > pyridine 1 > pyridine 2 groups.

The global reactivity parameters[24] such as the ionization potential ($IP = -E_{HOMO}$), electron affinity ($EA = -E_{LUMO}$), electronegativity ($\chi = \frac{(IP+EA)}{2}$), chemical potential ($\mu = -\chi$), chemical hardness ($\eta = \frac{(IP-EA)}{2}$), electrophilicity index ($\omega = \frac{\mu^2}{2\eta}$), and global softness ($S = \frac{1}{2\eta}$) are derived from the HOMO and LUMO energy values of the molecular structure and are given in Table 3. The ECT (electrophilicity-based charge transfer) approach and ΔN (charge transfer) parameters used to investigate the interaction between DNA bases such as adenine (AN), guanine (GN), cytosine (CN), and thymine (TN) and molecular structure are derived from the obtained reactivity parameters. In two interacting systems (A and B), ΔN and ECT parameters[22] can be given as $\Delta N = \frac{\mu_B - \mu_A}{2(\eta_A + \eta_B)}$ and $ECT = (\Delta N_{max})_A - (\Delta N_{max})_B = 2[\omega_A X_A - \omega_B X_B]$ $(X = \frac{1}{\chi})$. If the ECT value is negative, system A acts as a donor and the charge flow is $A \xrightarrow{charge\ transfer} B$. If it is positive, system B acts as an acceptor the opposite flow is $B \xrightarrow{charge\ transfer} A$.

Table 3. The global reactivity parameters of the $C_{22}H_{16}N_4O_2$.

$C_{24}H_{24}N_6OS_2$	B3LYP/6-311+G(d,p) Gas	B3LYP/6-311+G(d,p) Methanol	B3LYP/6-311+G(d,p) DMSO	B3LYP/6-311+G(d,p) Water
IP (eV)	6.09594	6.27119	6.27228	6.27336
EA (eV)	2.18591	2.37448	2.38210	2.38945
μ (eV)	−4.14093	−4.32284	−4.32719	−4.33141
χ (eV)	4.14093	4.32284	4.32719	4.33141
η (eV)	1.95502	1.94836	1.94509	1.94196
S (eV^{-1})	0.25575	0.25663	0.25706	0.25447
ω (eV)	4.38545	4.79556	4.81329	4.83046

Table 4. ΔN and ECT parameters (B: DNA bases, A: $C_{22}H_{16}N_4O_2$) obtained by using DFT/B3LYP/6-311+G(d, p) in water media.

	AN Base	GN Base	CN Base	TN Base	$C_{22}H_{16}N_4O_2$
Total Energy (a.u.)	−467.45	−542.72	−395.06	−453.59	−1217.75
IP (eV)	6.24	5.87	6.55	6.82	6.27
EA (eV)	0.81	0.42	1.00	1.13	2.39
μ (eV)	−3.52	−3.15	−3.78	−3.98	−4.33
χ (eV)	3.52	3.15	3.78	3.98	4.33
η (eV)	2.72	2.73	2.78	2.84	1.94
S (eV^{-1})	0.18	0.18	0.18	0.18	0.26
ω (eV)	2.29	1.82	2.57	2.78	4.83
ΔN	0.0869	0.1263	0.0583	0.0366	
ECT	0.4649	0.5555	0.4356	0.4170	

As can be seen from Table 3, the hardest methanol was found in the softest water environment for molecular structure solvent media. ΔN and ECT parameters determining the interaction between molecular structure and DNA bases are given in Table 4.

As can be seen from the ΔE and ECT values, a charge transfer can occur from DNA bases to the molecular structure. When the interaction is ordered from high to low impact, it is GN > AN > CN > TN.

UV-vis. spectra and magnetic studies of (HL) and (1)

The electronic spectrum of the **HL** (Figure 8) in DMSO (10^{-5} M) shows a band at 325 nm, which corresponds to n→π* transition of the carbonyl group. The π→π* transitions observed as a band and as a shoulder at 286 nm are assigned for the aromatic rings and azomethine moiety. In the electronic spectrum of the complex, the n→π* transition is higher wavelength shifted (325 nm to 385 nm, redshift) compared to the ligand. The presence of a broad band at 712 nm in the Cu(II) complex spectrum is the d-d transition band of the typical octahedral Cu(II) complex (Figure 9).[25,28,29]

In magnetic susceptibility measurements in a magnetic field, the paramagnetic complexes are attracted while the diamagnetic compounds repelled. Room temperature magnetic susceptibility measurement indicated paramagnetic nature for Cu complex. The observed magnetic moments for the Cu(II)

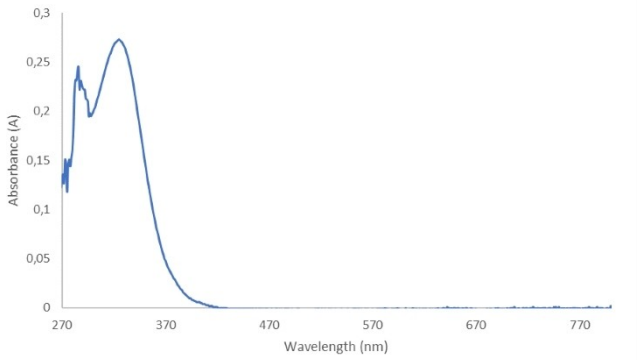

Figure 8. Absorption spectrum of the **HL**.

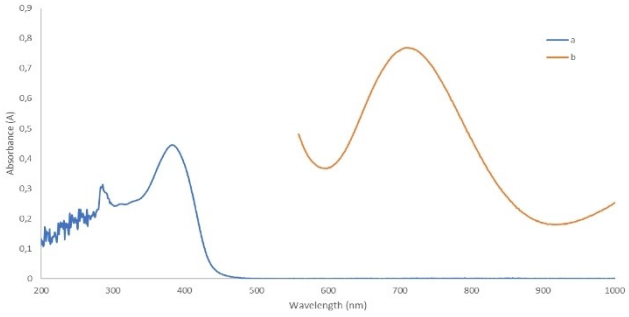

Figure 9. Absorption spectra of **1** a) 10^{-5} M, b) 10^{-2} M.

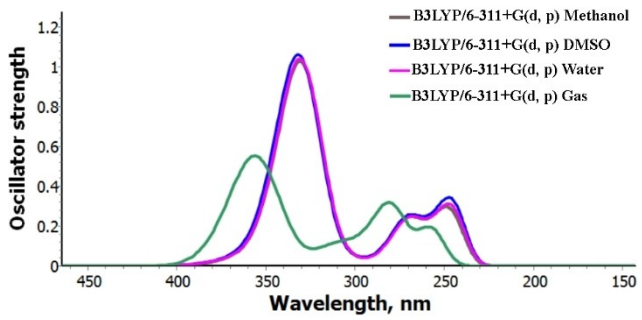

Figure 10. The theoretical UV-vis spectra of the molecular structure of the $C_{22}H_{16}N_4O_2$.

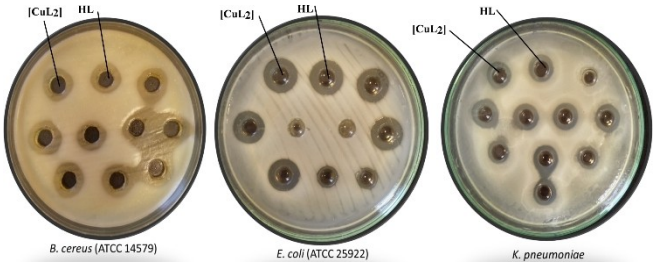

Figure 11. Image of antimicrobial zone diameters of **HL** and **1** on some pathogens.

complex is 1.78 B.M., suggesting a octahedral geometry around Cu(II).

The theoretical UV-vis spectra of the molecular structure were obtained from gas, methanol, DMSO, and water environments by the TD-DFT/B3LYP/6-311 + G(d, p) method. Table 5, it is given transitions of molecular orbital energy levels (for 20 states), percent distributions, absorption wavelengths, and oscillator stresses of the $C_{22}H_{16}N_4O_2$. The theoretical UV-vis spectra of the molecular structure are given in Figure 10. As can be seen from Figure and Table 5, absorption was observed at lower wavelengths in solvent media. The highest transition from the HOMO-1 level to the LUMO level occurred at approximately 330 nm and 280 nm with a probability of 96% and 69%, respectively.

Biological activity of (HL) and (1)

The antibacterial activity of the newly synthesized ligand and copper(II) complex was evaluated against different reference bacterial strains and clinical isolates using a liquid microdilution method. The results obtained showed that these compounds exhibited strong antimicrobial activity (Figure 11). C=N linkage is of particular importance in the biological activity of azomethine derivatives. In addition, the antibacterial effects of hydrazones can be achieved by increasing their chelating properties. These characteristics may be employed to transport metal across bacterial membranes or to adhere to bacterial cells at a precise location where it can obstruct their growth.[30–32]

The data presented in Table 6 show that between both novel compounds, the [CuL_2] complex has higher antibacterial activity compared to the HL. According to the results obtained, the tested compounds exhibited potent antimicrobial activity on both clinically important strains and on the type strains *E. coli* ATCC 25922, *P. aeruginosa* ATCC 27853, and *S. aureus* ATCC 25923. It is also noteworthy that the [CuL_2] complex has a low MIC value on these microorganisms. When the results of the compounds tested with gentamicin and streptomycin, which were used as positive controls in the study, are compared, it is seen that the MIC values are close. Overall, the data demonstrate that the test compounds have more potent antimicrobial activity on Gram-negative bacteria versus Gram-positive bacteria.

Conclusions

In this work, we reported the synthesis and characterization of a new 3-hydroxy-2-naphthoic hydrazide derivative hydrazone ligand **HL** and its Cu(II) complex. The structural characterizations of synthesized compounds were made by using elemental analysis, spectroscopic methods, LC–MS and magnetic measurements. The structure of **HL** was confirmed by ^{1}H-NMR. The ^{1}H-NMR signal of the NH group of the ligand was observed at 13.90 and the single signal of the OH group was observed at 11.28 ppm. From elemental analysis data, the metal-ligand ratio of the complexes was found to be 1:2. Magnetic moment measurement of the complex structure (1.78 B.M.) confirms that the structure has octahedral geometry.

Table 5. Transitions of molecular orbital energy levels (for 20 states), percent distributions, absorption wavelengths, and oscillator stresses (f) of the $C_{22}H_{16}N_4O_2$ (95th MO HOMO-1: H-1, 96th MO HOMO: H, 97th MO LUMO: L, and 98th MO LUMO + 1: L + 1).

TD-DFT	Wavelengths (nm) (% Distr.)	f	MO→MO	TD-DFT	Wavelengths(nm) (% Distr.)	f	MO→MO
6-311 + G	356(70%)	0.293	H-1→L	6-311G	332(96%)	1.060	H-1→L
(d, p)	313(62%)	0.068	H-3→L	(d, p)	280(69%)	0.280	H→L + 3
Gas	280(69%)	0.280	H→L + 3	DMSO	251(31%)	0.100	H→L + 4
	258(32%)	0.093	H-5→L				
6-311 + G	330(96%)	1.028	H-1→L	6-311G	331(96%)	1.040	H-1→L
(d, p)	271(62%)	0.171	H-1→L + 2 H→L + 5	(d, p)	271(64%)	0.161	H-1→L + 2
Methanol	250(29%)	0.107		Water	251(33%)	0.078	H→L + 5

Table 6. The antibacterial activity of the newly synthesized ligand and copper(II) complex.

Compounds	Antimicrobial zone diameters											
	Gram-negative						Gram-positive					
	E. coli 25922	*E. coli*	PA 27853	PA	KP	EA 1304	SD 11456b	LM 19115	*S. aureus* 25923	*S. aureus* (MRSA)	*B. cereus* 14579	*E. faecalis*
1	15±0.36	15±0.5	16±2.11	17±0.27	13±0.85	17±1.23	16±0.47	13±0.29	17±1.32	15±0.21	17±0.78	18±0.42
HL	12±1.27	13±1.56	n.d[b]	n.d	12±0.78	13±2.45	15±1.68	10±3.45	14±1.25	n.d	15±0.56	n.d
GN	19±0.11	18±0.34	15±0.28	16±0.32	18±0.58	21±0.56	19±0.32	n.d	18±0.52	19±0.47	23±0.14	n.d
CIP	22±1.52	24±0.75	25±1.02	27±1.36	22±0.47	18±0.21	21±1.22	n.d.	22±0.13	21±0.38	19±0.46	20±0.1
	MIC[a] (uM)											
1	32	16	8	16	8	8	16	64	8	16	32	8
HL	64	128	n.d[b]	n.d.	2	64	32	>256	64	64	8	n.d.
GN	1	2	1	2	1	0.5		n.d	1		2	n.d
CIP	0.5	0.5	1	0.5	0.5	2	0.5	n.d	0.5	1	0.5	0.5

[a] Minimum inhibitory concentration (MIC) was determined as the lowest concentration of peptide that inhibited bacterial growth determined in three independent experiments performed in triplicate. Abbreviations:PA: *P. aeruginosa*, KP: *Klebsiella pneumoniae*, EA: *Enterobacter aerogenes*, SD: *Shigella dysenteriae*, LM: *Listeria monocytogenes*, GN: Gentamisin, CIP: Siprofloksasin. [b] n.d: Not detected.

When the optimized molecular structures of **HL** were compared, a slight difference was observed in the bond parameters due to the different side groups. It can be said that **HL** is more stable in the water environment and is softer, that is, chemically active, in this environment. It was found from the MEP map that the carbonyl oxygen, hydrazine nitrogen, and pyridine nitrogen regions were at attractive potential and the naphthalene oxygen-hydrogen region was the repulsive potential region. It can be said that the highest contribution to the HOMO and LUMO energy levels comes from the atomic orbitals of naphthalene. Considering the interaction of **HL** with DNA bases, it can be said that the highest interaction is with the guanine base, and the guanine base acts as a donor, and the charge transfer is from the guanine base to the molecular structure. We can say that when DNA bases interact with **HL**, they can make intermolecular bonds with hydrazine, carbonyl and pyridine regions, which are the attractive potential regions of the molecular structure. In the experimental UV-vis spectra of **HL**, absorption wavelengths of 325 nm and 286 nm were observed versus n→π* and π→π* transitions in the DMSO medium. In the theoretical UV-vis spectra, results very close to the experimental values were obtained in the DMSO environment, 332 nm and 280 nm absorption wavelengths corresponding to the HOMO-1→LUMO and HOMO→LUMO + 3 transitions were obtained. Experimentally, d-d transitions of complex **1** were observed at absorption wavelengths of 712 nm.

When the antimicrobial activity of the newly synthesized ligand and its Cu(II) complex on clinically important isolates and pathogenic type strains was investigated, it was observed that the Cu(II) complex showed larger zone diameters on all tested microorganisms compared to the ligand. It is of great importance for clinical microbiology that it has more significant antimicrobial activity on Gram-negative bacteria compared to Gram-positive bacteria and its effective role on resistant microorganisms.

In studies, high antibacterial efficacy of copper (II) complexes was detected against clinical isolates of *Escherichia coli*, *Klebsiella pneumoniae*, *Enterobacter* spp., *Acinetobacter baumannii* and *Pseudomonas aeruginosa*. In our study, its antimicrobial activity was investigated on pathogens responsible for nosocomial infections and Gram-positive pathogens with multi-drug resistance, and it was found that it showed great antibacterial activity.

The fact that the tested compounds have strong antimicrobial activity on microorganisms such as *E. coli*, *P. aeruginosa* and *S. aureus*, which cause serious diseases in outpatient groups and cause death of intensive care patients, and resistant microorganisms such as MRSA, shows that they are compounds that may be alternative to antibiotics in the future. Also, the tested compounds have high antimicrobial activity against *E. faecalis*, a Gram-positive bacteria found in the gastrointestinal tract. The Cu(II) complex was found to have equal MIC values when compared to the reference compound gentamicin against *E. faecalis*. Comparing the antimicrobial activities of the new synthesis products with the antibiotics used as positive controls shows that the compounds can be an alternative to antibiotics. It is very important that the Cu(II) complex has an effect with a low MIC value. More research is needed in this area.

Experimental Section

Material and Methods

All chemicals used in this research were purchased from Sigma/Aldrich. All chemicals purchased from commercial suppliers were of reagent grade and were used without further purification. Thermo Flash 2000 Elemental Analyzer was used to record the elemental analyses. Thermo Evolution UV-visible Spectrophotometers operating between 200 and 1100 nm were used to record the electronic absorption spectra of the title chemical at room temperature in DMSO solution. Using an MXl Sherwood Scientific instrument magnet power supply, the Gouy method was used to measure the magnetic moments of the complexes. Thermo Scientific Nicolet iS10 FT-IR (Fourier Transform-Infrared) spectrophotometer was used to record IR spectra using ATR. In the DMSO solution, the mass spectra of the ligand and complex were captured. With the use of an Agilent Premium Compact 600 MHz spectrometer, the NMR

spectra was captured. Using a Thermo Scientific TSQ Quantum Access Max, mass spectra were collected (see Supporting Information).

Synthesis of (HL)

3-Hydroxy-2-naphthoic hydrazide (0.202 g, 1 mmol) was dissolved in methanol (20 mL). To this solution was added di-2-pyridyl ketone (0.183 g, 1 mmol) in methanol (20 mL). The mixture was refluxed for 4–5 h. The precipitated yellow product was filtered, washed repeatedly with ethanol, and dried in the air. Yield: 79%, Mp: 145°C; ^{1}H NMR (600 MHz, DMSO-d_6, ppm): $\delta = 13.90$ (s, 1H, NH), $\delta = 11.28$ (s, 1H, OH), $\delta = 7.48–8.86$ (m, 14H; Ar–H); FTIR (ATR, cm^{-1}): 3284 (NH), 3253 (OH), 1676 (C=O), 1628 (C=N)$_{azo}$, 1521 (C=N)$_{pyr.}$; UV-Vis. (DMSO, λ/nm): 286, 325; LC–MS (DMSO): *m/z* [found (calc.)]: 369.01 (368.13) (M + 1) (S1) ; elemental analysisi calcd (%) for $C_{22}H_{16}N_4O_2$: C 71.73, H 4.38, N 15.21; found: C 72.13, H 4.37, N 15.35. The chemical structure of **HL** is shown in Scheme 1.

Synthesis of (1)

A solution of $Cu(CO_2CH_3)_2 \cdot H_2O$ (0.199 g, 1 mmol) in methanol (10 mL) was added to a hot solution containing HL (0.736 g, 2 mmol) in methanol (20 mL). The reaction mixture was refluxed for 3–4 h. The precipitated brown product was filtered and dried in the air. Yield: 55%, Mp(decomp.): 285 °C. FTIR (ATR, cm^{-1}): 3233 (OH), 1638 (C=N)$_{azo}$, 1584 (> C N–N=C <), 1509 (C=N)$_{pyr.}$, 1362 (C–O); UV-Vis. (DMSO, λ/nm): 385, 712; LC–MS (DMSO): *m/z* [found (calc.)]: 799.18 (798.04) (M + 1) (S2) ; elemental analysisi calcd (%) for $C_{44}H_{30}N_8O_4Cu$: C 65.55, H 4.03, N 14.00; found: C 64.98, H 3.77, N 13.73. The chemical structure of **HL** is shown in Scheme 1.

Detection of antimicrobial activity

The antibacterial activity of the newly synthesized ligand and copper(II) complex was performed by the agar well diffusion method. In the study, *Escherichia coli* ATCC 25922, *Pseudomonas aeruginosa* ATCC 27853, *Staphylococcus aureus* ATCC 25923, *Bacillus cereus* ATCC 14579, *Listeria monocytogenes* ATCC 19115, *Enterobacter aerogenes* ATCC 1304 and *Shigella dysentery* ATCC in patients hospitalized in intensive care unit in the intensive care unit of Hospital clinical samples were used. These clinical strains are *Pseudomonas aeruginosa*, *Escherichia coli*, *Klebsiella pneumoniae*, *Enterococcus faecalis* and methicillin-resistant *Staphylococcus aureus* (MRSA). Tryptone Soy Broth medium (TSB) was used to develop clinical and type strains. In this method, 100 μl of the components with a concentration of 100 mg/ml were added to the wells of the agar plates, which were inoculated with 1 night-activated cultures and homogeneous distribution was achieved, and incubated at 37 °C for 24 hours. Antimicrobial activity was determined by measuring the inhibition zone diameter (mm).

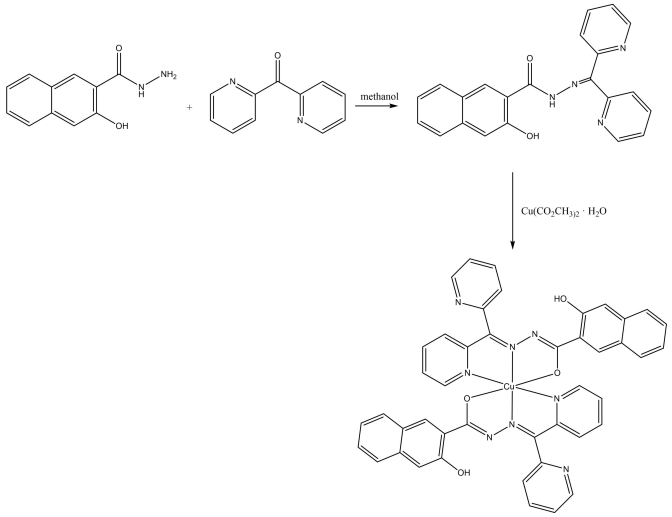

Scheme 1. Synthesis of HL and 1.

Determination of minimum inhibitory concentration (MIC)

The minimal inhibitory concentration (MIC) was determined using a modified standard of the Clinical and Laboratory Standards Institute (CLSI) broth microdilution method. Cultures developed in TSB medium at 37°C for 1 night were diluted to 1×10^6 CFU/mL. HL and 1 were dissolved in dimethyl sulfoxide (DMSO) and then diluted in 2-fold dilutions to a final concentration of 256–2 μM. Then, 50 μL of different concentrations of HL and 1 and an equal volume of bacterial suspension were added to the 96-well plate and incubated at 37 °C for 18 hours. The minimum concentration at which no visible bacterial growth occurred was defined as the MIC. Medium containing metal-free bacteria was used as a negative control, and gentamicin and ciprofloxacin (Sigma Aldrich, USA) were used as a positive control.[33]

Computational Details

The Gaussian 09 software[34] was utilized to analyze the HL's molecular structure. Theoretical computations were performed utilizing Density Functional Theory (DFT). The Hohenberg-Kohn and Khon-Sham approximations were used to construct the quantum mechanics-based computational chemistry technique known as DFT. Additionally, the Hamiltonian expression of a multi-electron system is calculated using this approach using the Born-Oppenheimer approximation. The computations employed the[35] basis function, one of the hybrid functions, to determine the exchange and correlation energy in the energy eigenvalue of a multi-electron system. The foundation set for these calculations was the diffuse-polarized 6-311 + G(d, p).

Supporting Information Summary

ThSupporting Information contains the MS data for HL and compound **1**.

Acknowledgements

The authors acknowledge to Central Research and Application Laboratory, Kırşehir Ahi Evran University. This work was supported by the Ahi Evran University Scientific Research Projects Coordination Unit. (Project Number: AHİLAB.A4.20.001).

Conflict of Interests

The authors declare no conflict of interest.

Data Availability Statement

The data that support the findings of this study are available in the supplementary material of this article.

Keywords: Aroyl hydrazone · Biological activity · Cu(II) complex · Schiff bases · DNA bases · 3-hydroxy-2-naphthoic hydrazide

[1] R.C. Moellering Jr., *Int. J. Antimicrob. Agents.* **2011**, *37 (1)*, 2–9.
[2] L. Popiołek, K. Paruch, P. Patrejko, A. Biernasiuk, M. J. Wujec, *Iran Chem Soc.* **2016**, *13*:1945–195.
[3] M.J. Ruben, M. Lehn, G. Vaughan, *Chem. Commun.* **2003**, 1338.
[4] L.H. Uppadine, J.-P. Gisselbrecht, J. M. Lehn, *Chem. Commun.* **2004**, 718.
[5] L.H. Uppadine, J.-M. Lehn, *Angew. Chem., Int. Ed.* **2004**, *43*, 240.
[6] A. Wood, W. Aris, D.J.R. Brook, *Inorg. Chem.* **2004**, *43*, 8355.
[7] S. Naskar, M. Corbella, A.J. Blake, S.K. Chattopadhyay, *Dalton Trans.* **2007**, 1150–1159.
[8] S. Rollas, Ş.G. Küçükgüzel, *Molecules* **2007**, *12,* 1910–1939.
[9] Y.-Q. Di, Y.-L. Liu, Y.-Y. Di, C.-S. Zhou, Y.-L. Ren, M.-Q. Li, *Chinese Journal of Structural Chemistry* **2018**, *37* (4), 557–563.
[10] C. Qiao, L. Sun, S. Zhang, Q. Wei, C. Zhou, G. Xie, S. Chen, X. Yang, S. Gao, *Polyhedron* **2016**, *119*, 445–450.
[11] S. Piotto, S. Concilio, L. Sessa, R. Diana, G. Torrens, C. Juan, U. Caruso, P. Lannelli, *Molecules* **2017**, *22*, 1372.
[12] S. Concilio, L. Sessa, A.M. Petrone, A. Porta, R. Diana, P. Iannelli, S. Piotto, *Molecules* **2017**, *22*, 875.
[13] Z. Li, L. Wu, T. Zhang, Z. Huang, G. Qiu, Z. Zhou, L. Jin, *Dalton Trans.* **2014**, *43*, 7554–7560.
[14] C. Gökçe, R. Gup, *Appl. Organometal. Chem.* **2013**, *27*, 263–268.
[15] M. Piscopo, M. Trifuoggi, C. Scarano, C. Gori, A. Giarra, F. Febbraio, *Sci. Rep.* **2018**, *8,:*7414.
[16] R. Diana, B. Panunzi, A. Tuzi, U. Caruso, *J. Mol. Struct.* **2019**, *1197*, 672–680.
[17] Ş. Karadeniz, C.Y. Ataol, O. Şahin, Ö. İdil, H. Bati, *J. Mol. Struct.* **2018**, *1161*, 477–485.
[18] O.A. El-Gammal, A.A. El-Bindary, F. S. Mohamed, G. N. Rezk, M. A. El-Bindary, *J. Mol. Liq.* **2022**, *346*, 117850.
[19] H. A. Kiwaan, A. S. El-Mowafy, A.A. El-Bindary, *J. Mol. Liq.* **2021**, *326*, 115381.
[20] O. A. El-Gammal, F. S. Mohamed, G. N. Rezk, A. A. El-Bindary, *J. Mol. Liq.* **2021**, *330*, 115522.
[21] K. S. Abou-Melha, G. A. Al-Hazmi, I. Althagafi, A. Alharbi, F. Shaaban, N. M. El-Metwaly, M. A. El-Bindary, *J. Mol. Liq.* **2021**, *334*, 116498.
[22] S. N. Shukla, P. Gaur, M. L. Raidas, B. Chaurasia, S. S. Bagri, *J. Mol. Struct.* **2021**, *1240*, 130582.
[23] L. Popiolek, K. Paruch, P. Patrejko, A. Biernasiuk, M. Wujec, *J. Iran Chem. Soc.* **2016**, *13*:1945–1951.
[24] M. Bakir, O. Green, W. H. Mulder, *J. Mol. Struct.* **2008**, *873*, 17–28.
[25] A. Ahmed, R.A. Lal, *Arabian J. Chem.* **2017**, *10*, S901–S908.
[26] Ç. Yüksektepe Ataol, *Erzincan University Journal of Science, Technology* **2022**, *5*, 592–608.
[27] M. Çınarlı, Ç. Yüksektepe Ataol, E. Çınarlı, O. Idil, *J. Mol. Struct.* **2020**, *1213*, 128152.
[28] J. Karpagam, N. Sundaraganesan, S. Sebastian, S. Manoharan, M. Kurt, *J. Raman Spectrosc.* **2010**, *41*, 53–62.
[29] T. E. Olalekan, D. R. Beukes, B. V. Brecht, G. M. Watkins, *J. Inorg. Chem.* **2014**, 769573.
[30] A. Z. El-Sonbati, M. A. Diab, A. A. El-Bindary, M. I. Abou-Dobara, H. A. Seyam, *Spectrochim. Acta Part A* **2013**, *104*, 213–221.
[31] G. A. Al-Hazmi, K. S. Abou-Melha, I. Althagafi, N. El-Metwaly, F. Shaaban, M. S. Abdul Galil, A. A. El-Bindary, *Appl. Organomet. Chem.* **2020**, *34*, e5672.
[32] M. A. El-Bindary, A. A. El-Bindary, *Appl. Organomet. Chem.* **2022**, *36*, e6576.
[33] C. Zhong, T. Liu, S. Gou, Y. He, N. Zhu, Y. Zhu, L. Wang, H. Liu, Y. Zhang, J Yao, J. Ni, *Eur. J. Med. Chem.* **2019**, *182*, 111636.
[34] M. J. Frisch, G. W. Trucks, H. B. Schlegel, G. E.Scuseria, M. A. Robb, J. R. Cheeseman, G. Scalmani, V. Barone, B. Mennucci, G. A. Petersson, H. Nakatsuji, M. Caricato, X. Li, H. P. Hratchian, A. F. Izmaylov, J. Bloino, G. Zheng, J. L. Sonnenberg, M. Hada, M. Ehara, K. Toyota, R. Fukuda, J. Hasegawa, M. Ishida, T. Nakajima, Y. Honda, O. Kitao, H. Nakai, T. Vreven, J. A. Montgomery, Jr., J. E. Peralta, F. Ogliaro, M. Bearpark, J. J. Heyd, E. Brothers, K. N. Kudin, V. N. Staroverov, R. Kobayashi, J. Normand, K. Raghavachari, A.Rendell, J. C. Burant, S. S. Iyengar, J. Tomasi, M. Cossi, N. Rega, J. M. Millam, M. Klene, J. E. Knox, J. B. Cross, V. Bakken, C. Adamo, J. Jaramillo, R. Gomperts, R. E. Stratmann, O. Yazyev, A. J. Austin, R. Cammi, C. Pomelli, J. W. Ochterski, R. L. Martin, K.Morokuma, V. G. Zakrzewski, G. A. Voth, P. Salvador, J. J. Dannenberg, S. Dapprich, A. D. Daniels, O. Farkas, J. B. Foresman, J. V. Ortiz, J. Cioslowski, D. J. Fox, **2009**, Gaussian 09, Wallingford (CT, USA): Gaussian, Inc.
[35] C. Lee, W. Yang, R. G. Parr, *Phys. Rev.* **1988**, *B37*, 785–789.

Manuscript received: August 24, 2023